813. Analysis of vibrations in a modeled ballasted track using measured rail defects

J. I. Real[1], T. Asensio[2], L. Montalbán[3], C. Zamorano[4]

[1, 2, 3] Department of Transportation Engineering and Infrastructures, School of Civil Engineering
Technical University of Valencia, 14 Camino de Vera, 46022 Valencia, Spain
[4] Foundation for the Research and Engineering in Railways, 160 Serrano, 28002 Madrid, Spain
E-mail: [1]*jureaher@tra.upv.es*, [2]*taasser@cam.upv.es*, [3]*laumondo@cam.upv.es*, [4]*claraz@fundacioncdh.com*

Abstract. Vibrations generated by trains and transmitted to the ground and nearby structures are a known source of problems associated with railway transport. Therefore this phenomenon should be studied in detail to avoid a negative impact on the environment. Within this framework, the article develops an improved version of a previously published analytical model capable of predicting ground vibrations caused by the passing railway vehicles. The new features include a new formulation of the models with five layers of material and an enhanced load input process that takes into account actual rail defects data as well as the Hertz theory for the rail-wheel contact. The model is adapted to a conventional ballasted track in Solares (Spain) as well as calibrated and validated with data collected on site. Hence the model is proved to be able to properly reproduce vibrations for the case of varying track typologies, constituting a useful research and design tool.

Nomenclature

a	Track gauge
A	Rail cross-sectional area
A_k	Rail shear cross-sectional area
c_2	Train primary damping coefficient
c_{Lj}	Rail pad/sleeper/ballast/ground 1/ground 2 longitudinal wave velocity (j = 1, 2, 3, 4, 5)
c_{Tj}	Rail pad/sleeper/ballast/ground 1/ground 2 shear wave velocity (j = 1, 2, 3,4 ,5)
C	Equivalent ballast coefficient
E	Rail and wheel Young's modulus
E_j	Rail pad/sleeper/ballast/ground 1/ground 2 Young modulus (j = 1, 2, 3, 4, 5)
E'	Hertz equivalent elastic modulus
G	Rail shear modulus
h_j	Layer thickness (j = 1, 2, 3, 4, 5)
I	Rail inertia in y-axis direction
k_1	Equivalent track spring constant
k_2	Train primary spring constant
K_H	Hertz contact stiffness
m_1	Unsprung mass per axle
m_2	Sprung mass per axle
P_i	Harmonic load magnitude
Q	Static load per axle
R_0	Hertz effective radius of curvature
R_R	Rail longitudinal radius of contact
R_{RT}	Rain transverse radius of contact
R_W	Wheel longitudinal radius of contact
R_{WT}	Wheel transverse radius of contact
V	Train velocity
y_1	Unsprung mass vertical displacement

880

y_2	Sprung mass vertical displacement
z_r	Rail vertical profile
α_1	First semi-axis of elliptical contact area
α_2	Second semi-axis of elliptical contact area
ε	Wheel roughness
λ_j	First Lamé parameter ($j = 1, 2, 3, 4, 5$)
$\lambda*_j$	First damping coefficient ($j = 1, 2, 3, 4, 5$)
μ_j	Second Lamé parameter ($j = 1, 2, 3, 4, 5$)
$\mu*_j$	Second damping coefficient ($j = 1, 2, 3, 4, 5$)
θ	Angle between planes containing R_w and R_R
ρ	Rail mass density
ρ_j	Rail pad/sleeper/ballast/ground 1/ground 2 mass density ($j = 1, 2, 3, 4, 5$)
υ	Rail and wheel Poisson coefficient
υ_j	Rail pad/sleeper/ballast/ground 1/ground 2 Poisson coefficient ($j = 1, 2, 3, 4, 5$)
$\overline{\omega_i}$	Harmonic load frequency
ξ	Hertz parameter

Introduction

The increasing development of both urban and interurban railway lines across the world is a consequence of growing mobility needs as well as rising environmental concerns among the citizenry. Railways present many advantages such as high capacity and low CO_2 emissions compared to other transport means. However, they also present certain potential problems which should be addressed in order to make this transport mean a truly beneficial choice.

Within this context, vibrations caused by the passing trains arise as one of the main sources of potential disturbance for the environment near railway lines. The generation and transmission of mechanical waves through the track and the ground is a phenomenon widely studied and yet not fully modeled, therefore representing a challenge for track designers.

In order to better understand this process, Salvador et al. [1] and Real et al. [2] developed an analytical model of the wave generation and transmission through the track infrastructure. This model was calibrated and validated with real data for both a high-speed ballasted track and a tram slab track, hence proving to be a useful tool for further research.

The main objective of this paper is to improve certain important aspects of its formulation and adapt the model to a conventional ballasted. The most important improvement is the implementation of the model constituting five layers of materials. Moreover the load modeling is further enhanced from previous versions as it now takes into account the actual rail defects measured on-site.

The paper is structured as follows: first of all a brief literature review is provided. Then the model development is explained, focusing mainly on all the modified aspects from previous published versions. A brief explanation of the data collection is then described, and finally the model is calibrated and validated with acceleration data measured on the Santander-Liérganes line operated by FEVE (Ferrocarriles Españoles de Vía Estrecha) in the north of Spain.

Modeling vibrations associated with railways has been a subject of study for many years. From a theoretical point of view, it is worth mentioning the work of Thompson [3], which deals with both vibration and noise. More practical studies have been carried out such as [4] and [5], focusing on different aspects of the phenomenon.

In terms of modeling, there are two main approaches: analytical and numerical. Several works regarding both modeling schemes are reviewed in [1] and [2] as a background for the model presented in this paper. Among them the reader may consult [6] and [4] as an example of numerical formulations and [7] and [8] as an example of analytical approaches.

881

The way loads are defined as an input for a vibration model has been widely addressed for numerical models ([9]) but it is still an issue when choosing an analytical formulation. The model defined in [2] presented an improvement in this aspect by formulating both harmonic and static loads and defining a set of loads so as to represent the train axle configuration. However, that approach showed certain limitations as there was no actual data available to define wheel and rail defects and the disused Zimmermann formulation to calculate the static component of railway vibrations. Moreover, the auxiliary quarter-car model adopted to calculate input forces relied on a parameter representing the "track stiffness" which was only roughly calibrated along with the main model damping parameters.

The modeling of the loads induced at the track-wheel contact has been widely studied for many years. One of the seminal works regarding this issue is that of Hertz, who defined a general theory of contact of elastic solids [10]. This theory has been extensively applied to the wheel-rail contact problem with some variations ([3] and [11]), and its soundness has been widely assessed [12]. Nowadays, numerical formulations are used in several investigations ([13] and [14]). However, the non-linear Hertz theory developed in [3] has been implemented in this paper due to its better fit to the analytical formulation presented.

Analytical model

The model presented in this paper follows the same formulation developed in [1] and [2]. The model considers a two dimensional cut (length and depth) consisting of the track and the ground underneath. It provides both vertical and longitudinal displacements and stresses induced by the applied loads.

The section studied in this paper is a conventional ballasted track with wooden sleepers, screw spikes and UIC 45 rails. This typology is adapted to the model domain as shown in Fig. 1.
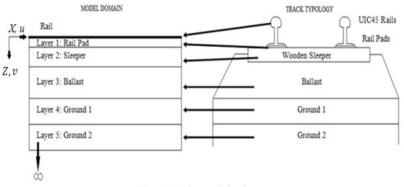

Fig. 1. Main model scheme

The new version of the model considers five layers to represent track behavior accurately. Layer 1 and layer 2 represent the rail pads and the sleepers respectively. These elements, which are discontinuous elements in the track, are made equivalent to the first and second layer by modifying its thickness so as to ensure a similar vertical behavior. The thicknesses of the layers in the model are calculated setting the vertical stiffness of the layer equal to the real stiffness of the elements. As a result, discrete elements will be transformed to continuous material layers.

This assumption may not work properly for horizontal displacements but it does for vertical ones and is accepted because vibrations in that direction are the most interesting for this study. As for the rails, they are modeled as a single Timoshenko beam of negligible thickness resting over the top layer.

The model core equation is the wave equation, expressed in vectorial terms:

882

$$(\hat{\lambda} + \hat{\mu})\nabla_{x,z}(\nabla_{x,z}\boldsymbol{d}) + \hat{\mu}\nabla_{x,z}^{2}\boldsymbol{d} = \rho\frac{\partial^{2}\boldsymbol{d}}{\partial t^{2}} \qquad (1)$$

where $\boldsymbol{d}$ is the displacement vector, ρ is the density of the material and $\hat{\lambda}$ and $\hat{\mu}$ are operators describing the viscoelasticity of the ground:

$$\hat{\lambda} = \lambda + \lambda * \frac{\partial}{\partial t}$$
$$\hat{\mu} = \mu + \mu * \frac{\partial}{\partial t} \qquad (2)$$

where λ and μ are Lamé parameters and $\lambda*$ and $\mu*$ are damping coefficients which must be calibrated using experimental data.

Load modeling

The load modeling is provided in order to obtain the forces, which applied to the model are made of a static component and some dynamic harmonic components. The objective is to generalize the inputs in the model. For this reason, both static and dynamic loads are modeled using harmonic loads with different amplitudes and frequencies:

$$F_{i}(t) = P_{i}\cos(\overline{\omega}_{i}t) \qquad (3)$$

where P_{i} represents the amplitude and $\overline{\omega}_{i}$ the harmonic load frequency of the i-th load F_{i}. The static load is considered as harmonic function with $\varpi = 0$ and P equal to the load applied by a single train axle, to represent that the static load is a permanent action. Each harmonic which represents dynamic loads is caused by certain rail or wheel defect such as rail joints, rail corrugations, wear and tear, etc.

In order to obtain the different pairs of amplitude and frequency to define the dynamic loads, an auxiliary quarter car model is used, as defined by [15]. The model layout, which represents a single train axle, is shown in Fig. 2.
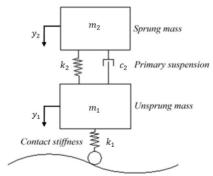

Fig. 2. Quarter car model scheme

The equations that describe the movement of the two masses are as follows:

$$m_{2}\frac{\partial^{2}y_{2}}{\partial t_{2}} + c_{2}(\frac{\partial y_{2}}{\partial t} - \frac{\partial y_{1}}{\partial t}) + k_{2}(y_{2} - y_{1}) = 0 \qquad (4)$$

883

$$m_1 \frac{\partial^2 y_1}{\partial t_1} - c_2 \frac{\partial y_2}{\partial t} + c_2 \frac{\partial y_1}{\partial t} - k_2 y_2 + (k_1 + k_2) y_1 - k_1 z_r = 0 \tag{5}$$

where z_r is the rail vertical profile, y_1 and y_2 are the vertical displacements of the unsprung and sprung masses respectively.

All the parameters in this quarter car model are known except for the track equivalent spring constant k_1. This parameter is calculated as the equivalent track stiffness, taking into account the wheel-rail contact stiffness:

$$\frac{1}{k_1} = \frac{1}{k_H} + \frac{1}{k_{rail}} + \frac{1}{k_{railpad}} + \frac{1}{k_{sleeper}} + \frac{1}{k_{ballast}} + \frac{1}{k_{ground}} \tag{6}$$

According to [3], the wheel-rail contact stiffness is due to local elastic deformation of both elements. As the contact area (which is assumed to be elliptical) depends on the load, this stiffness is not linear. The contact stiffness, K_H, depends on the geometry of the two bodies in contact, i.e. the rail and wheel. Curvature ratios in both the longitudinal and transverse direction are required, as shown in Fig. 3.
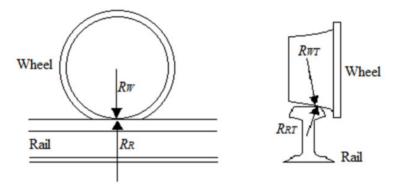

Fig. 3. Geometry parameters for the Hertz theory

These variables are used to define the following effective radius of curvature:

$$\frac{1}{R_0} = \frac{1}{2} \left(\frac{1}{R_W} + \frac{1}{R_{WT}} + \frac{1}{R_R} + \frac{1}{R_{RT}} \right) \tag{7}$$

Stiffness also depends on the material properties. Both wheel and rail are assumed to be made of the same steel, hence defining the following strain elastic modulus:

$$E' = \frac{E}{(1 - v^2)} \tag{8}$$

The angle between the planes containing R_W and R_R is defined as follows:

$$\cos \theta = -\frac{R_0}{2} \left(\frac{1}{R_W} - \frac{1}{R_{WT}} + \frac{1}{R_R} - \frac{1}{R_{RT}} \right) \tag{9}$$

Depending on the value of θ, non-dimensional parameter (ξ) is calculated. Its value was taken from a chart in [3] for the purpose of this paper. The reader may consult that reference for the precise mathematical definition of the parameters.

Now it is possible to calculate the Hertzian contact stiffness:

$$K_H = \frac{2E'\sqrt{R_0}}{3}\left(\frac{2}{\xi}\right)^{3/2} \tag{10}$$

The rest of values to calculate k_1, are obtained from [16].

Then, we can solve (4) and (5) and obtain the displacements y_1 and y_2 by means of a finite differences algorithm according to [15]. The expressions of the first and second order derivative in terms of finite differences are:

$$y' = \frac{y_{t+1} - y_t}{\Delta t} \tag{11}$$

$$y'' = \frac{y_{t+1} - 2y_t + y_{t-1}}{\Delta^2 t} \tag{12}$$

Introducing (11) and (12) in (4) and (5) and reorganizing:

$$y_{2_{t+1}} = \left(\frac{2m_2 - c_2\Delta t - k_2\Delta^2 t}{m_2}\right)y_{2_t} + \left(\frac{-m_2 + c_2\Delta t}{m_2}\right)y_{2_{t-1}} + \left(\frac{c_2\Delta t + k_2\Delta^2 t}{m_2}\right)y_{1_t} - \frac{c_2\Delta t}{m_2}y_{1_{t-1}} \tag{13}$$

$$y_{1_{t+1}} = \left(\frac{2m_1 - c_2\Delta t - (k_1 + k_2)\Delta^2 t}{m_1}\right)y_{1_t} + \left(\frac{-m_1 + c_2\Delta t}{m_1}\right)y_{1_{t-1}}$$
$$+ \left(\frac{c_2\Delta t + k_2\Delta^2 t}{m_1}\right)y_{2_t} - \frac{c_2\Delta t}{m_1}y_{2_{t-1}} + \frac{k_1\Delta^2 t}{m_1}z_t \tag{14}$$

This equation system may be solved iteratively using time increments from initial conditions, which does not affect to the final results due to the quick disappearance of its influence.

Once y_1 and k_1 are known, it is possible to calculate the forces at each point of the rail:

$$F_i = k_1(y_i - z_i) \tag{15}$$

The force function defined at Eq. (15) is plotted, yielding the force profile caused by rail defects. From this profile the main amplitudes and frequencies are taken, considering the train velocity, and feed the main model as different harmonic forces according to Eq. (3).

Model solution

Once the model equations and loads are defined, the following boundary conditions must be set. The horizontal displacement is u, v is the vertical displacement, σ_{xx} is the horizontal stress and σ_{xz} is the vertical stress. Note that these parameters depend on x, z and t, and the sub-index numbers express the layer where they are defined. According to [8], initial conditions are not required as only the stationary solution is to be calculated:

$$u_1(x,0,t) = 0 \tag{16a}$$

$$v_1(x,0,t) = w(x,t) \tag{16b}$$

$$u_1(x,h_1,t) = u_2(x,h_1,t) \tag{16c}$$

$$v_1(x,h_1,t) = v_2(x,h_1,t) \tag{16d}$$

$$\sigma_{ZZ_1}(x,h_1,t) = \sigma_{ZZ_2}(x,h_1,t) \tag{16e}$$

$$\sigma_{XZ_1}(x,h_1,t) = \sigma_{XZ_2}(x,h_1,t) \tag{16f}$$

$$u_2(x,h_1+h_2,t) = u_3(x,h_1+h_2,t) \tag{16g}$$

$$v_2(x,h_1+h_2,t) = v_3(x,h_1+h_2,t) \tag{16h}$$

$$\sigma_{ZZ_2}(x,h_1+h_2,t) = \sigma_{ZZ_3}(x,h_1+h_2,t) \tag{16i}$$

$$\sigma_{XZ_2}(x,h_1+h_2,t) = \sigma_{XZ_3}(x,h_1+h_2,t) \tag{16j}$$

$$u_3(x,h_1+h_2+h_3,t) = u_4(x,h_1+h_2+h_3,t) \tag{16k}$$

$$v_3(x,h_1+h_2+h_3,t) = v_4(x,h_1+h_2+h_3,t) \tag{16l}$$

$$\sigma_{ZZ_3}(x,h_1+h_2+h_3,t) = \sigma_{ZZ_4}(x,h_1+h_2+h_3,t) \tag{16m}$$

$$\sigma_{XZ_3}(x,h_1+h_2+h_3,t) = \sigma_{XZ_4}(x,h_1+h_2+h_3,t) \tag{16n}$$

$$u_4(x,h_1+h_2+h_3+h_4,t) = u_5(x,h_1+h_2+h_3+h_4,t) \tag{16o}$$

$$u_4(x,h_1+h_2+h_3+h_4,t) = u_5(x,h_1+h_2+h_3+h_4,t) \tag{16p}$$

$$\sigma_{ZZ_4}(x,h_1+h_2+h_3+h_4,t) = \sigma_{ZZ_5}(x,h_1+h_2+h_3+h_4,t) \tag{16q}$$

$$\sigma_{XZ_4}(x,h_1+h_2+h_3+h_4,t) = \sigma_{XZ_5}(x,h_1+h_2+h_3+h_4,t) \tag{16r}$$

$$u_5(x,\infty,t) = v_5(x,\infty,t) = \sigma_{ZZ_5}(x,\infty,t) = \sigma_{XZ_5}(x,\infty,t) = 0 \tag{16s}$$

Additionally, Eq. (1) is expressed in terms of the Lamé potentials so that vertical and horizontal displacements and stresses are as follows:

$$u = \frac{\partial \varphi}{\partial x} + \frac{\partial \psi}{\partial z}$$
$$v = \frac{\partial \varphi}{\partial z} - \frac{\partial \psi}{\partial x} \tag{17}$$

$$\sigma_{ZZ} = \hat{\lambda}\left(\frac{\partial^2 \varphi}{\partial x^2} + \frac{\partial^2 \psi}{\partial z^2}\right) + 2\hat{\mu}\left(\frac{\partial^2 \varphi}{\partial z^2} - \frac{\partial^2 \psi}{\partial x \partial z}\right)$$
$$\sigma_{XZ} = \hat{\mu}\left(2\frac{\partial^2 \varphi}{\partial x \partial z} - \frac{\partial^2 \psi}{\partial x^2} + \frac{\partial^2 \psi}{\partial z^2}\right) \tag{18}$$

Eq. (1) can be transformed in two scalar equations applying the Fourier Transform, as defined in Eq. (19):

$$\tilde{\tilde{f}}(k,z,\omega) = \int_{-\infty}^{\infty}\int_{-\infty}^{\infty} f(x,z,t) e^{i(\omega t - kx)} dx dt \tag{19}$$

This yields the following system of ordinary differential equations, which is expressed in the frequency and circular wave number domain (represented by $\approx$):

$$\left. \begin{array}{l} \dfrac{d^2\widetilde{\widetilde{\varphi}}}{dz^2} - R_L^{\,2}\widetilde{\widetilde{\varphi}} = 0 \\[4mm] \dfrac{d^2\widetilde{\widetilde{\psi}}}{dz^2} - R_T^{\,2}\widetilde{\widetilde{\psi}} = 0 \end{array} \right\} \tag{20}$$

Once solved Eq. (20), the Lamé potentials in frequency-wave number domain for each j layer can be expressed as:

$$\widetilde{\widetilde{\varphi}}_j = A_{j1}(k,\omega)e^{R_{Lj}z} + A_{j2}(k,\omega)e^{-R_{Lj}z}$$
$$\widetilde{\widetilde{\psi}}_j = A_{j3}(k,\omega)e^{R_{Tj}z} + A_{j4}(k,\omega)e^{-R_{Tj}z} \tag{21}$$

And the displacements and stresses in terms of (k,z,ω) are therefore as follows:

$$\widetilde{u}_j(k,z,\omega) = ik(A_{j1}(k,\omega)e^{R_{Lj}z} + A_{j2}(k,\omega)e^{-R_{Lj}z}) + R_{Tj}(A_{j3}(k,\omega)e^{R_{Tj}z} - A_{j4}(k,\omega)e^{-R_{Tj}z}) \tag{22a}$$

$$\widetilde{v}_j(k,z,\omega) = R_{Lj}(A_{j1}(k,\omega)e^{R_{Lj}z} - A_{j2}(k,\omega)e^{-R_{Lj}z}) - ik(A_{j3}(k,\omega)e^{R_{Tj}z} + A_{j4}(k,\omega)e^{-R_{Tj}z}) \tag{22b}$$

$$\widetilde{\sigma}_{zzj}(k,z,\omega) = C_{j1}(A_{j1}(k,\omega)e^{R_{Lj}z} + A_{j2}(k,\omega)e^{-R_{Lj}z}) + C_{j2}(A_{j3}(k,\omega)e^{R_{Tj}z} - A_{j4}(k,\omega)e^{-R_{Tj}z}) \tag{22c}$$

$$\widetilde{\sigma}_{xzj}(k,z,\omega) = D_{j1}(A_{j1}(k,\omega)e^{R_{Lj}z} - A_{j2}(k,\omega)e^{-R_{Lj}z}) + D_{j2}(A_{j3}(k,\omega)e^{R_{Tj}z} + A_{j4}(k,\omega)e^{-R_{Tj}z}) \tag{22d}$$

where:

$$\begin{aligned} C_{j1} &= (\widetilde{\lambda}_j + 2\widetilde{\mu}_j)R_{Lj}^{\,2} - \widetilde{\lambda}_j k \\ C_{j2} &= -2ik\widetilde{\mu}_j R_{Tj} \\ D_{j1} &= 2ik\widetilde{\mu}_j R_{Lj} \\ D_{j2} &= \widetilde{\mu}_j(k^2 + R_{Tj}^{\,2}) \end{aligned} \tag{23}$$

Boundary conditions in Eq. (15) can be also transformed to frequency and wave number domains using (19). Once converted to (k,ω) domain, they are taken into account to obtain an algebraic system whose variables are the different A_j coefficients. After solving, displacements and stresses for each layer are known in the frequency domain. The last step is to apply the inverse transform to obtain those variables in the time domain. This step is performed numerically as explained in [2]. The resulting vertical displacement is derived twice to obtain vertical accelerations. The resulting acceleration is shifted accordingly to the axles' configuration to obtain the full accelerogram at a specific point of the model domain caused by the passing of the whole train.

Both the main model and the auxiliary quarter car model were implemented in Mathematica® 7.0 (Wolfram Research Inc.).

Model calibration

The formulated model is now calibrated with actual data collected from the railway track located in Solares (Cantabria, Spain). In this way, damping coefficients for each layer (λ_j^*, μ_j^*) are obtained. Calibration is carried out by the root mean square difference method between the

actual and modeled accelerations as defined by [17]. The RMSD between the real accelerogram $a_{z_r}(t)$ and the modeled accelerogram $a_{z_m}(t)$ is obtained as:

$$RMSD = \sqrt{\frac{\sum_T (a_{z_r}(t) - a_{z_m}(t))^2}{\sum_T (a_{z_r}(t))^2}} \qquad (24)$$

The value of RMSD represents the mean error between the actual and the modeled accelerations. In our calibration, the criterion to accept a solution is a mean error of 5 %.

Acceleration data collection

Data gathered for model calibration and validation was measured on-site in a rather straight track stretch of the Santander-Liérganes line in Cantabria, Spain. This line is operated by FEVE and consists on a conventional ballasted track with UIC 45 rails and wooden sleepers. The track gauge is 1 meter.
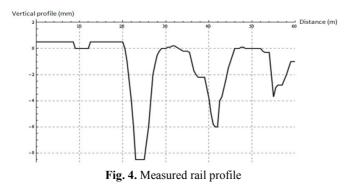
Three Sequoia FastTracer® triaxial accelerometers based on MEMS technology were used to measure accelerations on the track. Two were placed on the top surface of two non-consecutive sleepers and one on the rail foot. The characteristics of the sensors are shown in Table 1.

Table 1. Accelerometers characteristics

	Sensors on sleepers	Sensor on rail
Scope	±5g	±18g
Bandwidth (Hz)	0-2500	0-2500
Resolution (m/s^2)	0.041	0.13
Noise (m/s^2)	0.075	0.093
Sampling rate (Hz)	8192	8192

Acceleration at those three points was registered for several trains passing through the studied section within a week. The data obtained was exported to Mathematica® 7.0 (Wolfram Research Inc.) in order to process and compare them with the model output for calibration and validation.

As for the rail profile, it was measured by means of a ballast tamping and lining machine provided by ACCISA. Measurements were carried out at night to avoid any interruption of the train regular service. Fig. 4 shows the rail profile along a 60-meter track stretch.

Fig. 4. Measured rail profile

The line is operated by a single vehicle class: the CAF S/3800 consisting on three carriages and six bogies. Technical data including masses, damping and geometry was provided by FEVE.

888

Velocity at the monitored section was recorded by the drivers and provided afterwards, giving a mean speed of 25 km/h.

Discussion of results

In this section the results given by the model are discussed. First of all, Fig. 5 shows the comparison between modeled and measured accelerations on the surface (i.e. over the sleeper) after calibration. Calibrated parameters are listed in Table 2.

Table 2. Model parameters after calibration

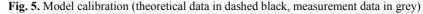| Parameter (Pa)	Layer 1	Layer 2	Layer 3
$\lambda*$	No influence		
$\mu*$	450 000	400 000	525 000

From the figure it is clear that the model gives a good approximation of the measured accelerogram. Consecutive peaks of acceleration due to the passing of the train axles are reproduced, and the time of growing and decay of the signal is also similar. Therefore, calibration criteria are met (values are shown in Table 3) and the model is successfully calibrated.

Table 3. Calibration criteria

Criteria	Model	Data	Difference
Maximum peak (m/s^2)	75	74	1
Absolute minimum peak (m/s^2)	78	63	15
Growth (s)	0.5	0.9	0.4
Decay (s)	1.7	1.5	0.2

From Fig. 5 it is clear that the modeled accelerogram is much 'cleaner' than the measured one. This is due to the fact that measurements include vibrations caused by several rail and wheel defects as well as certain resonance components (e.g. the rail pad or the fastening screws) that the model does not consider. This is particularly clear when looking at the growing part of the accelerogram, as the measured one takes more time of growth and shows many small, secondary peaks not reproduced by the model. The main reason for this difference is that only a few harmonics were obtained from the rail profile shown in Fig. 4 (mainly those due to rail joints) and fed to the main model, and thus there are many other defects not considered including those of the wheels. Transient effects are also not reproduced as the model only yields a stationary solution.

Fig. 5. Model calibration (theoretical data in dashed black, measurement data in grey)

However, despite this limitation, the model reproduces the main trends of the measured accelerogram because the response due to the quasi-static load is dominant compared to the dynamic ones for the velocity considered (i.e. about 25 km/h). A better reproduction of the dynamic components of the vibration wave (which would be more important for greater velocities) only requires more comprehensive data of the wheel and rail defects so as to feed the model with more harmonic loads.

Another noteworthy issue is the difference of concordance between model and data for positive and negative peaks. The model as formulated is fairly symmetrical and yields rather similar maximum and minimum values. The data, on the other hand, is quite asymmetrical as there is a difference of about 10 m/s^2 between peaks. It is unclear why the measurements show such trend, and thus the model has been calibrated to fit higher peaks despite overestimating lower ones so as to be on the safer side.

Regarding the calibrated parameters, damping coefficient $\lambda*$ was found to be irrelevant when modeling vertical displacements, a result which confirms the observation made in [2]. This parameter has influence on the horizontal displacements, but those are not considered for the purpose of this paper because of the lack of data and the assumed hypothesis of continuous sleepers previously described.

Damping coefficient $\mu*$, on the other hand, has a great influence in the model output. As the data for calibration was only measured in the sleepers, only the first parameter μ_1* is fully calibrated. However, the other two parameters do have an impact in the vibration wave modeled and thus are also calibrated to certain extent. This difference from the behavior shown in [2] is due to the different track typology studied. This ballasted track is far less rigid than the slab track studied in the previous paper (note the damping coefficients are two orders of magnitude lower than those obtained in [2]) and the behavior of each layer affects the others to a greater extent.

The calibrated model was then validated with a different set of data. The results are shown in Fig. 6 and the validation criteria are presented in Table 4.
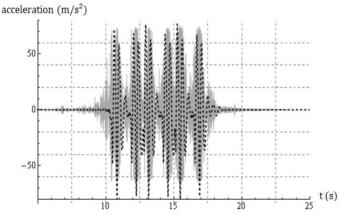

Fig. 6. Model validation (theoretical data in dashed black, measurement data in grey)

Table 4. Validation criteria

Criteria	Model	Data	Difference
Maximum peak (m/s^2)	76	72	4
Absolute minimum peak (m/s^2)	79	63	16
Growth (s)	0.6	1.5	0.9
Decay (s)	1.7	2.2	0.5

Once again the model overestimates negative peaks but reproduces quite well the positive ones. This is an acceptable result as was explained previously. The wave main traits are correctly predicted and thus the model is properly validated.

Finally, in order to test the model performance across the entire domain, Fig. 7a and Fig. 7b shows modeled accelerations in the ballast layer (Fig. 7a) and the ground 1 (Fig. 7b) at 0.2 and 0.5 meters of depth respectively. When compared with the accelerogram modeled at the surface (Fig. 5 and Fig. 6), a clear alleviation of the wave with depth can be pointed out. Peaks of acceleration are reduced from 76 to 30 m/s^2 (60 %) when the wave moves from the sleeper to the ballast and drop to 1.5 m/s^2 (98 %) when it reaches the ground. This behavior shows that the model is capable of simulating vibration mitigation within its domain and thus it can be used to study wave propagation through different track elements.
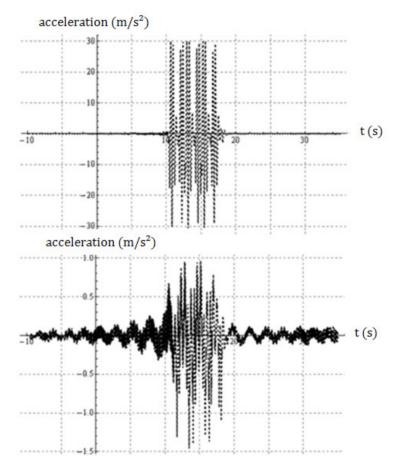

Fig. 7. Modeled accelerations: 7a: at the ballast layer (depth: 0.2 m); 7b: at the ground layer (depth: 0.5m)

Conclusions

The paper has presented and improved version of the previously developed and reported analytical model and has applied it to a conventional ballasted track in Solares, Spain. The model has been calibrated and validated using actual data measured on site.

The five-layer model has been implemented and it has been proven to more accurately represent the track behavior. The improvements made regarding load modeling have proved to

891

work properly as the model reproduces the measured wave fairly accurately. In addition, the inclusion of the non-linear Hertz theory provides the model a sounder theoretical base and simplifies the calibration process by reducing the number of parameters to be adjusted.

The model still has certain limitations that should be taken into account. The actual phenomenon of vibration transmission through a track infrastructure is made of several static and dynamic components and the model is only capable of reproducing a portion of them. Transient phenomena and resonance of singular elements such as rail pads or fastening systems are not included in the model formulation. Heterogeneity of the ground and ballast layer is not considered, and singular track features cannot be studied. On the other hand, the improved load modeling allows including virtually every dynamic load due to wheel and rail defects providing there is accurate data available.

This may be another limitation as accurate data is not always available or easy to obtain. However, as the results have proven, for the velocity considered the main features of the wave are properly reproduced with only a few components (i.e. pairs of frequency/amplitude) of measured rail defects. Therefore, the model can yield a good approximation of the phenomenon even with a reduced source of data.

Considering the results obtained in this paper as well as those shown in [1] and [2], the model developed represents a useful tool to study vibration propagation through different track infrastructures, from conventional and high-speed ballasted tracks to urban slab tracks. Therefore, it can be used by designers to assess the vibration performance of new and existing tracks as well as to model the first stage of vibration transmission within wider research projects related to the effects of train-induced vibrations for the environment.

Acknowledgements

Appendix. Values of the parameters used in the study

Table 5. Values of the parameters used in the study

Parameter	Value
m_1	3.445 Tn
m_2	7.305 Tn
k_2	47.48 kN/mm
c_2	26000 N/m$\cdot$s^{-1}
k_{rail}	7.35$\cdot$10^6 kN/m
$k_{railpad}$	6.56$\cdot$10^5 kN/m
$k_{sleeper}$	6.5$\cdot$10^5 kN/m
$k_{ballast}$	2$\cdot$10^5 kN/m
k_{ground}	1$\cdot$10^5 kN/m
R_W	0.425 m
R_{WT}	0.6 m
R_R	∞
R_{RT}	0.305 m

References

[1] **Salvador P., Real J., Zamorano C., Villanueva A.** A procedure for the evaluation of vibrations induced by the passing of a train and its application to real railway traffic. Mathematical and Computer Modeling, Vol. 53, Issue 1-2, 2010, p. 42-54.

[2] **Real J. et al.** Modeling vibrations caused by tram movement on slab track line. Mathematical and Computer Modeling, Vol. 54, Issue 1-2, 2011, p. 280-291.

[3] **Thompson D. J.** Railway Noise and Vibration: Mechanisms, Modeling and Means. Oxford (UK): Elsevier, 2009.

[4] **Sheng X. et al.** Prediction of ground vibration from trains using the wavenumber finite and boundary element methods. Journal of Sound and Vibration, Vol. 293, Issue 3-5, 2006, p. 575-586.

[5] **Jones C. J. C. et al.** Simulations of ground vibration from a moving harmonic load on a railway track. Journal of Sound and Vibration, Vol. 231, Issue 3, 2000, p. 739-751.

[6] **Yang Y. B., Hung H. H.** Soil vibrations caused by underground moving trains. Journal of Geotechnical and Geoenvironmental Engineering, Vol. 135, Issue 3, 2008, p. 455-458.

[7] **Koziol P. et al.** Wavelet approach to vibratory analysis of surface due to a load moving in the layer. International Journal of Solids and Structures, Vol. 45, Issue 7-8, 2008, p. 2140-2159.

[8] **Metrikine A. V., Vrouwenvelder A. C. W. M.** Surface ground vibration due to a moving train in a tunnel: two-dimensional model. Journal of Sound and Vibration, Vol. 234, Issue 1, 2000, p. 43-66.

[9] **Auersch L.** The excitation of ground vibration by rail traffic: theory of vehicle–track–soil interaction and measurements on high-speed lines. Journal of Sound and Vibration, Vol. 284, Issue 1-2, 2005, p. 103-132.

[10] **Hertz H.** Contact of Elastic Solids. Miscellaneous Papers. London (UK): Macmillan & Co. Ltd., 1896.

[11] **Otero J.** Study of rail vehicle dynamics in curved tracks. Part I: Wheel-rail contact analysis. Revista Colombiana de Tecnologías de Avanzada, Vol. 14, Issue 2, 2009, p. 48-53.

[12] **Yan W., Fischer F. D.** Applicability of the Hertz contact theory to rail-wheel contact problems. Archive of Applied Mathematics, Vol. 70, Issue 4, 2000, p. 255-268.

[13] **Kalker J. J.** Three Dimensional Elastic Bodies in Rolling Contact. Dordrecht (Netherlands): Kluwer Academic, 1990.

[14] **Polach O.** A fast wheel-rail forces calculation computer code. Vehicle System Dynamics, Vol. 33 (Supplement), 1999, p. 728-739.

[15] **Melis M.** Introducción a la dinámica vertical de la vía y señales digitales en ferrocarriles. Madrid (Spain): Escuela de Ingenieros de Caminos Canales y Puertos, 2008.

[16] **López A.** Infraestructuras Ferroviarias. Barcelona: Cenit, 2006.

[17] **Arslan Y. Z. et al.** Prediction of externally applied forces to human hands using frequency content of surface EMG signals. Computer Methods and Programs in Biomedicine, Vol. 98, Issue 1, 2010, p. 36-44.